All-natural superhydrophobic coating for packaging and blood-repelling materials

Juling Li [a], Juanhua Tian [b], Yingtao Gao [a], Rongrong Qin [a], Hemu Pi [a], Mengjie Li [a], Peng Yang [a],[*]

[a] *Key Laboratory of Applied Surface and Colloid Chemistry, Ministry of Education, School of Chemistry and Chemical Engineering, Shaanxi Normal University, Xi'an 710119, China*
[b] *Department of Urology, The Second Affiliated Hospital of Xi'an Jiaotong University, West Five Road, No. 157, Xi'an 710004, China*

ARTICLE INFO

ABSTRACT

The design of a bio-safe superhydrophobic coating to repel water adsorption, food and blood adherence is significantly important to attenuate food spoilage, food waste and thrombi. Herein, we synthesize an all-natural superhydrophobic interfacial material that has strong interfacial stability on a variety of substrates, and has good repellence towater, highly-viscous liquid foods and biofluids (blood, urine, etc.). The base material is simply prepared in an aqueous solution of lysozyme and cysteine, in which the rapid phase transition of lysozyme is triggered by a cysteine-induced thiol-disulfide exchange reaction. The resulting phase-transited lysozyme (PTL) aggregates into microparticles with a nanoscale roughness, which are further packed into a dense layer with a micro-/nano-topography. The PTL is composed of an inner amyloid-like structure and shows strong interfacial adhesion with the underlying substrate due to amyloid-inspired adhesion. The PTL layer is finally converted to a robust coating to effectively repel liquid foods and biofluids by being decorated with a natural hydrophobic carnauba wax. This coating noticeably enhances the water repellence of cellulose-based packaging materials, and the resulting superhydrophobic paper is completely non-wetted by water without weakening the mechanical stability and usability of the modified paper. The coating further resists the adhesion of milk, yogurt, honey and various other beverages and edible liquids, which leaves no residue on the coated surface. This coating also significantly resists wetting by blood and other human biofluids with a noticeable decrease in platelet adhesion on the surface. This work underlines the importance of an amyloid-like protein assembly in the preparation of an all-natural green interfacial coating towards the robust repellence of water, edible liquids and blood.

1. Introduction

Inspired by superhydrophobic surfaces in nature e.g., lotus leaves, duck feathers [1–4], the non-wettablity of a superhydrophobic surface towards water, liquid food and biofluids facilitates a wide range of applications such as self-cleaning [5–10], anti-fogging [11], and anti-icing [12–14], along with biomedicine [15–17], and oil-water separation [18,19]. The two main factors for constructing a superhydrophobic interface are the rough micro-/nano-structure and particular hydrophobic components with low surface energy. While both top-down and bottom-up methods have been utilized to construct micro-/nano-structures on a surface [20–25], current hydrophobic components are largely constrained to fluoroalkanes, as they can provide long-term hydrophobic stability [26–29]. However, long-chain fluorocarbon materials are generally regarded as a non-degradable toxic contaminants with

notorious safety concerns for humans and ecosystems [30], thereby making these materials difficult to be used in the fields of commodities, food packaging and medicine. In this regard, it is very important to develop a bio-safe, non-toxic superhydrophobic material with good degradability and cost-effective scale-up [31]. Ideally, to synthesize such a material, it should meet several requirements. 1. The solvent and reactants used in the experiment should be non-toxic or be volatile without leaving any residue in the material. 2. The method to construct a superhydrophobic surface must be simple, recyclable, low-cost and fast to meet the standard of a scaled-up industrial fabrication and should be able to be formed on various material surfaces with a variety of structures and shapes [32]. Although recent studies have shown the potential to use fatty acids (e.g., cinnamic acid, myristic acid) and natural wax (e. g., bee wax, candelilla wax and rice bran wax) as fluoroalkane alternatives [33–37], the biggest problem of these materials is that the

hydrophobic effect of these components is not as good as that of fluoroalkanes, especially in a long-term duration. For instance, the adhesion force between these natural substances and a substrate is extremely weak, which easily results in the detachment of the hydrophobic component or the entire coating from the substrate, thus becoming a well-recognized unsolved challenge to hinder a practical application of natural superhydrophobic materials [38]. Moreover, traditional coating methods are typically applicable only on planar substrates, and it is challenging to construct a superhydrophobic coating on a substrate with complex non-flat shapes such as the interior spaces of tubes and bags [15,39]; thus, their real-life application is severely limited.
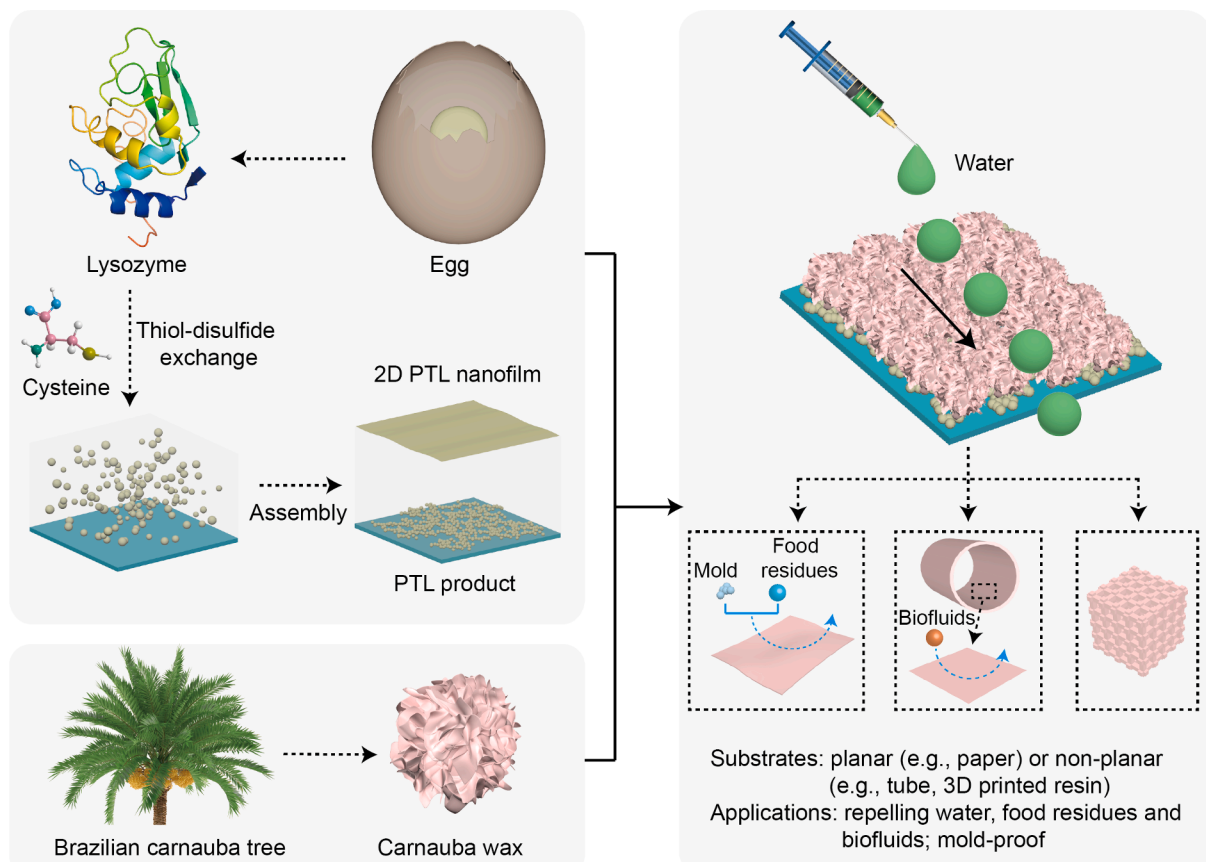
In the present work, inspired by the lotus leaf that contains cellulose (providing the mechanical properties and macropapillae) and wax nanocrystals (hydrophobic component) [31], we synthesize a superhydrophobic coating that simultaneously combines natural bio-safety with good interfacial adhesion stability on virtually arbitrary surface, mechanical robustness, and long-term non-wettability to water, edible liquids and biofluids (e.g., blood and urine). A key natural resource in this work is lysozyme (lys), an antibiotic enzyme extracted from egg white and commercially available at a low price. A fast phase transition of lysozyme can be stimulated by a non-toxic reducing agent, in this case, cysteine (cys). The thiol-disulfide exchange reaction is triggered to prepare a phase-transited lysozyme (PTL) nanofilm at the air/water interface and a PTL product in the solution (Fig. S1) [40–42]. In this process, cysteine could selectively reduce the Cys6-Cys127 disulfide bond of lysozyme to trigger the spontaneous α-helix to β-sheet transition of proteins (Fig. S2) [40]. The resultant amyloid-like aggregates including PTL nanofilm and product with micro-/nano-scale topography, could attach to a variety of substrate surfaces due to amyloid-like structure-mediated interfacial adhesion [40–44]. Subsequently, the PTL nanofilm and product are coated further by carnauba wax, being approved by the U.S. Food and Drug Administration (FDA) as an edible

substance and extracted from the leaves of Brazilian carnauba tree, to achieve the facile production of a superhydrophobic material in a green, energy-saving, and low-cost process (Scheme 1). The resultant superhydrophobic surface noticeably enhances the water repellence of cellulose-based materials (e.g., paper) and their resistance to mold without compromising their mechanical stability and usability. In addition to pure water, the superhydrophobic coating further resists the adhesion of a wide range of food residues (e.g., milk, yogurt, honey and beverages as well as other edible liquids) and biofluids (e.g., blood and urine) with a noticeable decrease in platelet adhesion on corresponding surfaces. The competitive advantage of this method is further highlighted by showing its capability to easily coat non-flat substrates (e.g., the interior spaces of tubes and 3D-printed resin). Furthermore, this superhydrophobic coating is non-toxic to mammalian cells and exhibits robust interfacial interactions that improve the mechanical and superhydrophobic stability of the coating on a variety of substrates due to the co-contribution of the supramolecular interactions. Therefore, the method and corresponding materials in this study are highly useful for developing recyclable packaging materials and biocompatible blood-contacting materials.

2. Experiment section

2.1. Materials

Lysozyme (extracted from egg white) was purchased from Sigma-Aldrich or Shanghai yuanye Bio-Technology Co., Ltd. Carnauba wax and cysteine were obtained from Aladdin. Sodium diphenyl diazobis-α-naphthylamine-4-sulfonate (Congo red), phosphate buffered saline (PBS), artificial saliva, gastric juice, body fluid, urine, 4-(2-hydroxyethyl)-1-piperazineethanesulfonic acid (HEPES) buffer (pH = 7.2 ~ 7.4) and fluorescein isothiocyanate labeled bovine serum albumin (BSA-

Scheme 1. Schematic illustration of the formation and applications of the all-natural superhydrophobic surface.

FITC) were purchased from Beijing Solarbio Co., Ltd. All fermented milk, drinks, honey, soy sauce and vinegar were purchased from the local supermarket. The fresh blood was taken from New Zealand White Rabbit. Hydrogen peroxide (H_2O_2), dimethyl sulfoxide (DMSO), sodium hydroxide (NaOH), n-hexane and sulfuric acid (H_2SO_4) were purchased from Sinopharm Chemical Reagent Co. Ltd. Aspergillus niger (A. niger) (ATCC16404), mouse fibroblast (3T3) cells were obtained from American Type Culture Collection (USA). Heparin sodium was purchased from Dalian Meilun Biotechnology Co., Ltd. Potato Dextrose Agar (PDA) was purchased from Guangdong Huankai Microbial Sci. & Tech. Co., Ltd. Dulbecco's modified eagle medium (DMEM) was purchased from Hyclone. Ultrapure water was used in all experiments and supplied by Milli-Q Advantage A10 (Millipore, USA). The silicon (Si) wafer and flat glass were cleaned with Piranha solution (concentrated H_2SO_4: 35% H_2O_2 = 7:3 v/v) at 90 °C for 5 h (Caution: Piranha solution reacts violently with organic materials; it must be handled with extreme care, followed by copious rinsing with ultrapure water). The magnesium (Mg), copper (Cu) and titanium (Ti) wafer were ultrasonic cleaning with ethanol after polishing the surface. The polyvinyl chloride (PVC), polypropylene (PP), polyimide (PI), polyethylene glycol terephthalate (PET), polycarbonate (PC), low density polyethylene (LDPE) and yogurt lid were rinsed with copious ethanol.

2.2. Preparation of the all-natural superhydrophobic coating

The lysozyme phase transition buffer (equivoluminal of 14 mg/mL lysozyme and 14 mg/mL cysteine with pH 10, both of which were dissolved in 10 mM of HEPES buffer) was dropped on the substrate (including metals, glass, silicon, plastics and paper) and incubated for 2 h at room temperature. By this process, a robust phase-transited lysozyme (PTL) product coating was acquired.

Carnauba wax (6 mg) and n-hexane (1 mL) were mixed and then heated to dissolve. Then, the protein-based superhydrophobic interface was obtained by the spin coating of the hot wax solution onto the surface of the PTL product at the speed of 3000 rpm.

2.3. The stability of the superhydrophobic coating

For the abrasion durability, the all-natural superhydrophobic surface was placed face-down to a sandpaper (grit no. 240 or 400) under the weight of 200 g slider and moved for the distance of 6 cm. In this way, the coefficient of static friction (μ) was obtained. The maximum static sliding friction (F_f) could be calculated by:

$F_f = \mu*F_N$ (F_N is the gravity of the slider)

For the bending durability, the superhydrophobic surface was constructed on the PET, and cut into rectangle shapes (specification was 1*5 cm), then it was bent for different times with 180° bending angle.

For the dynamic flushing durability, the protein-based superhydrophobic coating (the substrate was glass) was placed under water at a flow rate (Q) of 6.25 mL/s (375 g/min) for different duration. The impact force (F) could be calculated by theorem of momentum:

$$Ft = mv_2 - mv_1 \ (v_2 = 0) \tag{1}$$

$$v_1 = Q/S \tag{2}$$

$$m = \rho V \tag{3}$$

$$V = Qt \tag{4}$$

Available from (1), (2), (3), $F = \rho Q v_1$.

m is the mass of the water; V is the volume of water impacted on the surface in a short time (t); S is the cross-sectional area of the water flow; v_1 and v_2 are the initial and final velocity of the water flow respectively; ρ is the density of water.

2.4. Hemolysis assay

A superhydrophobic coating was prepared on PET. 12 cm^2 of the modified PET was then immersed in physiological saline and incubated in an oven at 37 °C for 72 h. After centrifugation, the supernatant was obtained as the extract. Fresh rabbit blood supplemented with heparin sodium was centrifuged at 3000 rpm for 5 min, and the underlying substance was configured as 2% red blood cells. Add red blood cells to the extract, and use ultrapure water and physiological saline as positive and negative controls, respectively. After the above samples were incubated at 37 °C for 1 h, the absorbance at 545 nm was measured. The formula to calculate the hemolysis ratio is:

$$HR = \frac{A - B}{C - B} \times 100\%$$

HR is the hemolysis ratio of the experimental sample, %; A, B, C are the absorbance values of the experimental group, the negative control group (no red blood cells rupture observed in normal saline), and the positive control group (the rupture of red blood cells resulting in the release of large amounts of hemoglobin in ultrapure water), respectively.

2.5. Platelet adhesion assay

Fresh rabbit blood supplemented with heparin sodium was centrifuged at 1000 rpm for 10 min, and the upper platelet-rich plasma (PRP) was added to the surface of the samples. The samples were incubated at 37 °C for 1 h and then rinsed slightly with saline. And then, the samples were dehydrated with 50, 70, 90, 100% ethanol after overnight fixation with 1% glutaraldehyde.

2.6. Aspergillus niger growth on the superhydrophobic paper

Aspergillus niger was added to the sterilized Potato Dextrose Agar and cultured for 24 h. The Aspergillus niger solution was then added on the superhydrophobic paper and blank paper respectively followed by the incubating for 1, 2, 3 days at 27 °C. The sample was then fixed with 1% glutaraldehyde (prepared with 1 × PBS) for 24 h, and then dehydrated with 50, 60, 70, 80, and 90% ethanol.

2.7. The cytotoxicity evaluation of the all-natural superhydrophobic coating

The cell viability of 3T3 cells was measured by the tetrazolium bromide reduction (MTT) assay for the superhydrophobic material. Typically, the 6 cm^2 modified glass was immersed in 1 mL DEME medium at 37 °C for 24 h to obtain the extract. The cells were inoculated in different media [blank DMEM medium and DMEM medium containing different concentrations of extract (6, 3, 1.5, 0.75 cm^2/mL)] with a cell density of 3000 cell/cm^2. After cultivation for 24, 48, 72 h, 90 μL of fresh DMEM medium and 10 μL of MTT solution were added to the 96-well plate and then incubated for another 3 h. Finally, the MTT/DMEM solution was replaced with DMSO for color development, and the absorbance at 490 nm was detected with a spectrophotometric microplate reader.

2.8. The BSA-FITC adsorption on the superhydrophobic coating

The superhydrophobic surface was covered with 1 mg/mL BSA-FITC solution and incubated at room temperature for 30 min, 2 h, and 12 h, respectively. The surface was then rinsed with ultrapure water and subjected to the characterization.

2.9. Characterization

Scanning electron microscopy (SEM) was conducted on FEI Quanta

200 electron microscope (SU8020, Hitachi) with the primary electron energy of 5 kV. The fluorescence spectrum was collected by an F-7000 fluorescence spectrophotometer (Hitachi). Atomic force microscopy (AFM) was performed by CSPM 5500 (MultiMode, NanoScope IV from Benyuan Inc, China) in tapping mode. Fourier transform infrared (FTIR) spectra were recorded on a Tensor 27 (Bruck). The UV/vis spectrum was collected by U-3900/3900H (Hitachi). The Raman spectrum was collected using an in Via Reflex (Renishaw) with 785 nm laser excitation. Water contact angle (WCA) measurements were performed by an interface/tensiometer (DCAT 21 and OCA 20, Dataphysics, Germany). X-ray photoelectron spectroscopy (XPS) was obtained with AXIS ULTRA from Kratos Analytical Ltd., the binding energies were calibrated by setting C_{1s} peak at 284.6 eV. Water vapor permeance was obtained with i-HYDRO 7310 Water Vapor Permeation Analyzer (Labthink). The cell
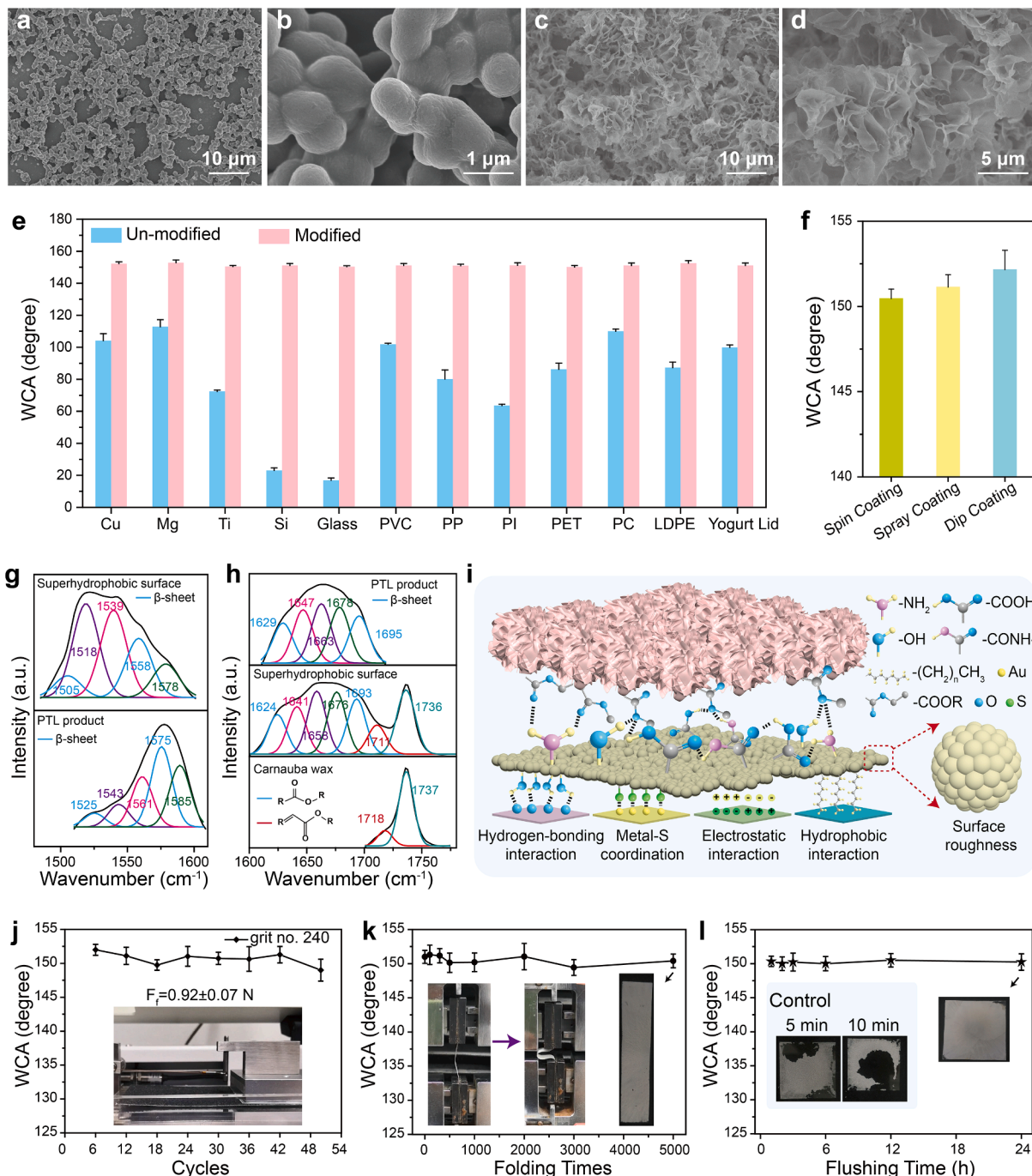

Fig. 1. (a, b) Scanning electron microscopy (SEM) images of the PTL product. (c, d) SEM images of the PTL product coated with carnauba wax. (e) WCA on a variety of material surfaces before and after superhydrophobic modification. (f) WCA of the all-natural superhydrophobic surface prepared by different wax coating methods. (g) Deconvolution of the FTIR amide II peak of the superhydrophobic surface and the PTL product. (h) FTIR characterization of the PTL product, superhydrophobic surface and carnauba wax. (i) Schematic illustration of the supramolecular interactions inside the superhydrophobic surface. (j) WCA after rubbing the superhydrophobic surface for different times with sandpaper (grit no. 240). (k) WCA on the superhydrophobic surface after different folding cycles. The inset shows the folding angle at 180° and the superhydrophobic surface after folding 5000 times. (l) WCA on the superhydrophobic surface after flushing with water for different durations. The inset shows the carnauba wax coating without PTL as the intermediate layer (control) flushed for 5 min (left) and 10 min (middle), and the right inset shows the superhydrophobic surface flushed for 24 h (as indicated by an arrow).

viability assay was performed by Synergy Neo 2 Multi-Mode Reader (Gene).

3. Results and discussion

3.1. Preparation of the all-natural superhydrophobic coating

Typically, the phase transition solution was prepared by mixing lysozyme (14 mg/mL) and cysteine (14 mg/mL) in 10 mM (4-(2-hydroxyethyl)-1-piperazineethanesulfonic acid) (HEPES) buffer (pH 10). After incubating this solution on a solid surface for 2 h at room temperature, the PTL layer basement with a micro-/nano-scale topography was obtained [40]. The corresponding scanning electron microscopy (SEM) images showed that the PTL product layer had a network structure composed of microparticles with a nanoscale roughness ($\approx$1 µm in diameter, Fig. 1a, b). The corresponding thickness of the PTL product layer was approximately 10 µm according to the cross-sectional SEM image (Fig. S3). After the PTL product layer was modified by carnauba wax, a flower-like morphology was observed with a thickness of approximately 8 µm (Fig. S3); this morphology was formed by n-hexane evaporation-induced wax molecular self-aggregation (Fig. 1c, d) [35]. After this treatment, an all-natural-based superhydrophobic interface was acquired that showed a water contact angle (WCA) above 150°. The concentration of lysozyme and cysteine significantly affected the size of the microparticles, resulting in the following sizes: 500 nm at 7 mg/mL, 1 µm at 14 mg/mL, 2.4 µm at 28 mg/mL, and 3.5 µm at 56 mg/mL (Fig. S4). In addition to the concentrations of lysozyme and cysteine, the amount of wax used for the coating was also related to the superhydrophobic state. For a PTL layer surface with an area of 324 cm^2, coating with 200 µL or less of the wax solution was not enough to fully cover the entire PTL surface to produce the superhydrophobic state. Alternatively, volumes above 200 µL (e.g., 300 µL) of the wax coating solution could completely cover the PTL layer surface to attain a superhydrophobic state; notably, a further increase in the wax solution volume did not significantly change the multiscale structure and corresponding WCA (Fig. S5). Based on the above optimization, the superhydrophobic surface could be easily formed on virtually arbitrary material surface, including metals (Cu, Mg, Ti, etc.), inorganics (glass, Si), and polymers [polyvinyl chloride (PVC), polypropylene (PP), polyimide (PI), polyethylene glycol terephthalate (PET), polycarbonate (PC), low density polyethylene (LDPE), yogurt lid] (Fig. 1e). In addition to spin-coating of wax layer, other commonly used methods in industry, namely, spray and dip coating of wax, could also effectively produce a superhydrophobic state (Fig. 1f, Fig. S6), showing great potential for scaled-up fabrication.

The Fourier transform infrared (FTIR) spectra further reflected the successful coating of PTL on the substrate and carnauba wax on the PTL (Fig. S7a–c). The spectra of the superhydrophobic surface showed the characteristic peaks at 1656 and 1544 cm^{-1} for the amide I and II peaks of the protein in the PTL as well as 1736 and 1173 cm^{-1} for the stretching vibrations of the C═O and C–O–C of the ester groups in carnauba wax, respectively. In addition, the peaks at 2918 and 2850 cm^{-1} on the superhydrophobic surface indicated the stretching vibration of the –CH$_2$– in carnauba wax. It was found that the peak positions in the FTIR spectra for the amide band of the superhydrophobic surface were different from those for the PTL product layer. Notably, the amide II (representing the bending vibration of –NH–) peak at 1581 cm^{-1} of the PTL was shifted to 1544 cm^{-1} for the superhydrophobic coating (Fig. S7d). Furthermore, the original β-sheet aggregate peaks in the PTL layer before the wax coating were observed at 1525 and 1575 cm^{-1}, which clearly red-shifted to 1505 and 1558 cm^{-1} after coating with the wax (Fig. 1g). The other functional groups, such as –COOH, amide III (representing the stretching vibration of C–N) and –OH/–NH$_2$ of the PTL at 1300, 1468 and 3419 cm^{-1}, respectively, red-shifted to 1296, 1465 and 3279 cm^{-1} on the superhydrophobic surface, respectively (Fig. S7d, e). Carnauba wax is predominantly comprised of aliphatic esters

(–COOC–) and diesters of cinnamic acid (–C═C–COOC–) [45], which were further reflected by the peak positions in the deconvolution of the FTIR spectra at 1737 and 1718 cm^{-1}, respectively (Fig. 1h). The C═O of –C═C–COOC– (with abundant electrons obtained from π-π and p-π conjugation) clearly red-shifted from 1718 cm^{-1} for carnauba wax to 1711 cm^{-1} for the superhydrophobic surface (Fig. 1h). The above results implied that hydrogen bonds were possibly formed between the PTL (–CONH–, –COOH, –OH/–NH$_2$) and wax layers (–C═C–COOC–), since hydrogen bonding would average the electron cloud density to result in a redshift of the FTIR peaks of these functional groups from the PTL and carnauba wax (Fig. 1i) [46]. The hydrogen bonding between the PTL product and carnauba wax could also be supported by X-ray photoelectron spectroscopy (XPS) (Fig. S8), in which the binding energy for O, N and S of the superhydrophobic surface shifted noticeably to 531.7, 399.8 and 163.4 eV from the original 531.1, 399.6, 163.2 eV before the wax coating, respectively [47]. In addition, the peeling force of superhydrophobic surfaces constructed on the different thickness of PTL product layer controlled by different concentration of lysozyme and cysteine (3.2 µm for 7 mg/mL, 10.2 µm for 14 mg/mL, 35.6 µm for 28 mg/mL, and 70.4 µm for 56 mg/mL, Fig. S9) were studied. According to the cross-sectional SEM images of superhydrophobic surface after the 180° peeling test, the PTL product of 7, 14, 28 mg/mL was completely remained on the substrate without peeling off (Fig. S10). Therefore, the peeling force between the PTL product and the carnauba wax (14 mg/mL, 1028 N/m) was obtained which was 2.8 times higher than the carnauba wax with the glass (373 N/m) due to the formation of the hydrogen bonding interactions (Fig. S11).

The deconvolution of C, N, O, and S in the high-resolution XPS spectra of the superhydrophobic surface and PTL product layer also indicated that there were a variety of functional groups exposed on the surface, typically including thiols (C–S), aliphatic carbon (C–H/C–C), amines (C–N), hydroxyls (C–O), amides (O═C–N) and carboxyl groups (O═C–O) (Fig. S8c, d). Similarly, the corresponding Raman spectra and related amino acid residue analysis also reflected the existence of these functional groups on the PTL (Fig. S12). In a previous report, it was proven that the PTL assemblies could adhere well to different substrates due to the multiple bonding modes between the versatile functional groups of the PTL and the underlying substrate (Fig. 1i). These interactions might include an M-S (M stands for metal) coordination with thiol groups in the PTL, a hydrogen bonding/electrostatic interaction by the –NH$_2$ and –COOH from the PTL as well as the hydrophobic interaction between the PTL and the substrate. The versatile chemical structure offered by the amyloid product thus provided a multiple binding model that is universally applicable to various kinds of materials [44]. The co-contribution of these interactions allows the product to stably adhere to the surface of the material. The peeling force of the PTL product at different thickness was further studied. After 180° peeling, the PTL product prepared by 7 or 14 mg/mL of lysozyme still existed on the substrate, which indicated the phenomenon of peeling might occur between the tape/coating and the peeling force between the PTL product and glass was above 1232 N/m (Fig. S13). In contrast, the PTL product could be peeled off from the substrate with the maximum peeling force of 883 N/m for 28 mg/mL of lysozyme and 693 N/m for 56 mg/mL of lysozyme respectively. To further test the mechanical stability of the coating, the superhydrophobic surface was placed between a sandpaper with different roughness and a 200 g slider that was moved a distance of 6 cm to produce enough external friction [48]. The results reflected that the surface could resist the friction by the sandpapers (grit no. 240 and 400) with friction values of 0.92 and 0.78 N, respectively, for at least 50 times (Fig. 1j, Fig. S14, Movie S1). The bending test was used to further evaluate the mechanical stability of the coating in practical use. For this test, the coating was grown on a PET film, followed by being cut into rectangular shapes (specification was 1*5 cm) and bending at different times with a 180° bending angle (inset of Fig. 1k). The results indicated that the WCA of these surfaces did not decrease after being bent at least 5,000 times (Fig. 1k). Furthermore, the

superhydrophobic coating on glass was subjected to strong water flushing at a flow rate of 6.25 mL/s with a force of $1.05*10^{-2}$ N for different durations. After 24 h of scouring, the coating was still stable on the surface of the glass, and the WCA was maintained at approximately 150° (Fig. 1l). In contrast, more than half of the pure carnauba wax coating without PTL as the intermediate layer was washed away within 10 min (inset of Fig. 1l). The above mechanical stability tests reflected that common rubbing, bending or dynamic flushing by water that are typically experienced in daily uses would not significantly compromise the superhydrophobic property of the coating. Moreover, the robust coating without obvious peeling indicated the excellent interfacial adhesion and stability (comparing with the previous reports, Tables S1–S3) from the method and related materials in this study. In addition, the coating also exhibited thermo-stability because when the coating on glass was placed at 30–90 °C, the WCA remained as high as 150° (Fig. S15). In addition, the superhydrophobic coating could maintain its superhydrophobic state after the surface was immersed in the different kinds of organic solvents (dichloromethane, ethanol, ethyl ether, ethyl acetate, n-hexane and acetone) and the different pH solution (pH = 12, 2) for 2 h (Fig. S16).

3.2. The application of wax@PTL coating in packaging materials

The all-natural-based superhydrophobic coating in this study shows considerable promise for use in recyclable packaging materials. As one of the most important indispensable packaging materials, non-degradable plastics not only contribute large amounts of pollution to the environment but also exhaust valuable non-renewable fossil energy in large quantities. Therefore, the development of degradable, environmentally compatible and renewable materials has received increasing attention [49,50]. Cellulose is a major type of recyclable material; however, its ability to easily absorb water is an intrinsic weakness [51]. Paper, as a typical cellulose-based material (Fig. 2a, Fig. S17a), is largely used in human society and can easily absorb water, resulting in mechanical deformation and a damaged structure [52]. In the present work, a paper (printing paper or filter paper) surface could
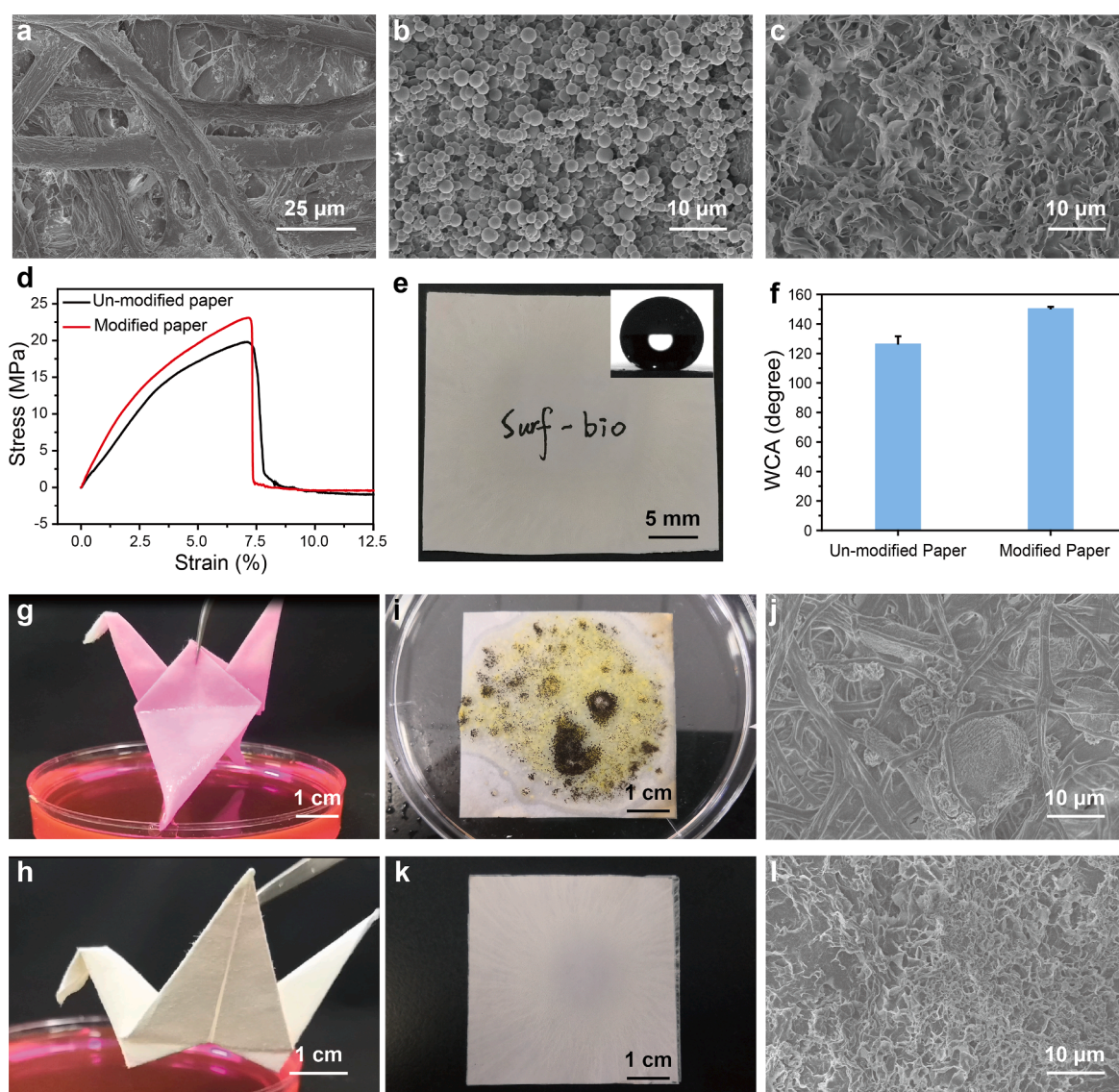

Fig. 2. SEM images of the (a) un-modified printing paper, (b) PTL product-coated printing paper, and (c) superhydrophobic printing paper with the wax@PTL coating. (d) Stress-strain curve of the un-modified paper and superhydrophobic paper. (e) Image showing the writing behavior on the superhydrophobic paper. (f) WCA on the un-modified and modified paper. Photos for the (g) un-modified and (h) superhydrophobic filter paper origami after being removed from dyed water (rhodamine B). (i) Optical picture and (j) corresponding SEM image of the un-modified paper after cultivating Aspergillus niger. (k) Optical picture and (l) corresponding SEM image of the superhydrophobic paper after cultivating Aspergillus niger.

be quickly modified by the as-prepared wax@PTL coating (Fig. 2b, c S17 b, c). Furthermore, the introduction of the wax@PTL coating would not compromise the original mechanical and writing properties of the paper (Fig. 2d, e). The superhydrophobic coating protected the paper well from the wetting of water, since the resultant WCA was changed from 126° on blank paper to 150° on the modified paper (Fig. 2f). Moreover, when an origami from blank filter paper was soaked completely in water dyed with rhodamine B, the origami quickly deformed and collapsed after removal due to water adsorption (Fig. 2g). In contrast, the origami

from superhydrophobic filter paper could not be soaked in water so as to maintain its original shape well without any water residue (Fig. 2h, Movie S2). The resultant water vapor transmission [WVT, 38 °C, 90% relative humidity (RH)] through the paper also consequently decreased by 26% compared with that of blank paper (Fig. S18). Furthermore, the water resistance was favourable for inhibiting bacterial growth on the paper. Paper is easily infected by mold, especially in humid environments because it provides a large amount of polysaccharides as nutrients to the mold. After 3 days of cultivating Aspergillus niger (a common type
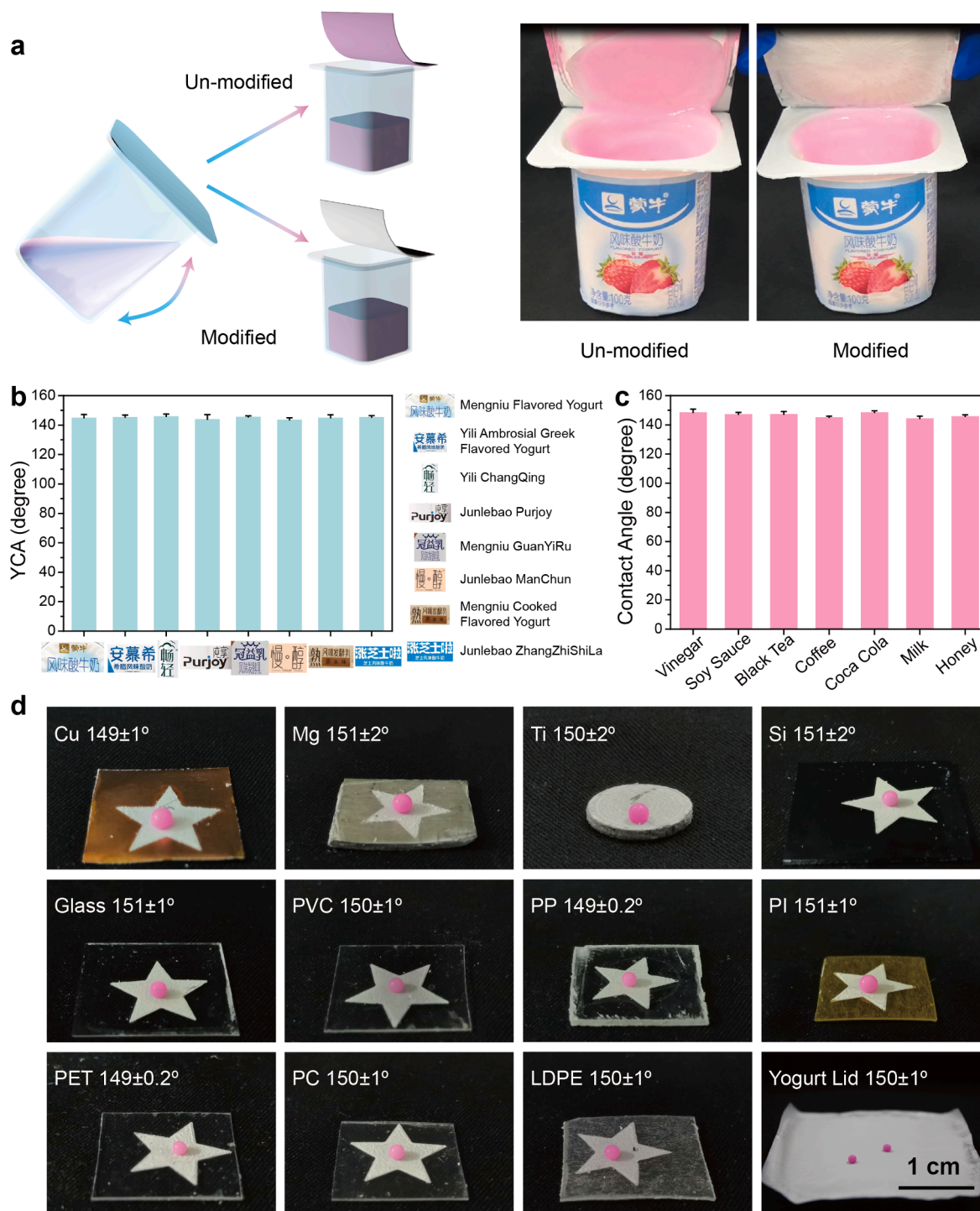

Fig. 3. (a) Yogurt residues on the modified and un-modified yogurt lid after shaking the yogurt box (yogurt was dyed with rhodamine B). Contact angles of different kinds of (b) yogurts and (c) food residues on the superhydrophobic surface. (d) Dyed yogurt droplets deposited on various substrates with the super-hydrophobic coating.

of mold) on unmodified and superhydrophobic paper, no Aspergillus niger growth was detected on the superhydrophobic paper, while a large amount of Aspergillus niger gradually proliferated on the blank paper over time (Fig. 2i–l, Fig. S19a, b). Moreover, after three days of Aspergillus niger cultivation, the modified superhydrophobic paper continued to maintain its superhydrophobic ability (Fig. S19c).

Thus, the above results suggest that the protein-based superhydrophobic coating has great application prospects for resolving the ineffective water resistance of recyclable materials. The wax@PTL coating was then utilized to tackle the issue of food residue on packaging materials as another challenge in food packaging materials. In daily life, significant waste is produced by residual liquid foods with certain viscosities adhering to their containers after they are poured out, such as fermented milk, honey and beverages [34]. This situation also makes it difficult to separate recyclable packaging materials from food in garbage classification, thereby increasing the burden of cleaning the packaging materials with valuable water and energy. In this regard, the creation of bio-safe and degradable food packaging materials that are able to autonomously separate food from the packaging material surface is particularly important. Thus, the wax@PTL coating was utilized to resist the adhesion of various food residues on packaging materials. First, modified and un-modified yogurt lids were resealed on a yogurt container, and there was no residual yogurt on the modified yogurt lid after shaking the yogurt box (Fig. 3a, Movie S3). In contrast, the un-modified lid showed a large amount of adhered yogurt. The yogurt contact angle (YCA) of different brands of fermented milk with various dynamic viscosities (Table S1) were all approximately 150° (Fig. 3b, Fig. S20). Among these yogurts, Ambrosial Greek Flavored Yogurt yogurt and Junlebao ZhangZhiShiLa (two yogurt brands) were more likely to stick on packaging materials because of their higher dynamic viscosities than other brands of yogurt. Nonetheless, the sliding angles for these yogurts remained low, with values of 20–24° for Ambrosial Greek Flavored Yogurt and Junlebao ZhangZhiShiLa as well as 12–16° for other yogurt brands (Fig. S21a). As a result, all of the tested yogurts could easily roll off the superhydrophobic surface without leaving behind residue (Movie S4). In addition to yogurts, a variety of liquid foods, such as vinegar, soy sauce, black tea, coffee, milk and even highly viscous honey (1407 mPa·s), also had contact angles above 148°, and the sliding angles of honey and other food products were 30° and less than 10°, respectively (Fig. 3c, Fig. S21b, S22). As a result, all of these foods could easily roll off the superhydrophobic surface (Movies S5). Furthermore, a variety of food packaging materials could then be modified by the wax@PTL coating to introduce a non-wetting state for liquid foods. A patterned star-shaped superhydrophobic coating was successfully fabricated on virtually any substrates such as metals (Cu, Mg, Ti), inorganics (Si, glass) and polymers (PVC, PP, PI, PET, PC, LDPE, yogurt lid) (Fig. S23). On these surfaces, the yogurt droplets exhibited the shape of small balls with YCA greater than 148° (Fig. 3d), showing a sharp contrast to the YCA on un-modified materials (Fig. S24). In addition, to further explore the release of the carnauba wax, the FTIR spectra of yogurt reflected that there was no characteristic absorption of ester groups in the yogurt after the superhydrophobic surface was fully in touch with yogurt for 24 h. Therefore, the release of the carnauba wax did not occur in the yogurt (Fig. S25). To better apply the superhydrophobic coating to the outer packaging of yogurt, the hydrophobic stability was further studied. The superhydrophobic state was not compromise after upside down the yogurt container for 24 h, the coating faced-down the yogurt for 5 days and shaking the container for 48 h (Fig. S26).

3.3. The application of wax@PTL coating in human-related issues

The successful application in food packaging materials may imply the expanded potential of the wax@PTL coating in more human-related functions. In this regard, the resistance to biofluid adherence on the wax@PTL coating is further tested. After applying a variety of human

secretory fluids (artificial saliva, gastric juice, body fluid and blood plasma) on the superhydrophobic surface, the contact angles of these biofluids were all approximately 150° (Fig. 4a). A practical application was then designed to use the superhydrophobic material as a toilet coating. When human urine was peed to the wax@PTL coating on a toilet for three times, it was found that there were no urine droplets on the superhydrophobic surface, while many urine droplets were observed on the tape next to the coating (Fig. 4b). Additionally, the superhydrophobic state of the coating remained effective even after scouring the coated surface with artificial urine for 30 times at an angle of 120° (Fig. 4c). In addition to resistance to urine adhesion, maintaining a non-wetting state with blood is especially useful in medical devices. When medical devices get in touch with blood, blood adherence on the surface could cause some adverse reactions, such as platelet adhesion and activation, leading to blood clots, thrombi, inflammation and so on [15]. Additionally, blood adhesion on a surface would induce significant blood loss in the container and transfusion tube [17]. In contrast to the blood contact angle (BCA) of nearly 20° on a blank glass surface, the wax@PTL superhydrophobic surface had a BCA of 150° with a sliding angle of 10° (Fig. 4d). This non-wetting state for blood allows the blood to easily roll off surface without leaving any blood residue (Fig. 4d inset, Movie S6).

3.4. The biocompatibility of the wax@PTL coating

Encouraged by the above result, the biocompatibility of the wax@PTL coating was further evaluated by the hemolysis test (GB/T 16175–2008, GB/T 16886.12–2017/ISO 10993–12:2012) and compared with the requirement for medical implants. This test detects the release of hemoglobin caused by the rupture of red blood cells when blood is in contact with the superhydrophobic surface. The corresponding sample and negative control (saline solution) then showed the nearly overlapping absorption curve in the UV–vis spectra to present a low hemolysis ratio (HR) at 1.19%, indicating good blood compatibility without significant hemolysis for the wax@PTL coating (Fig. 4e). In addition, carnauba wax did not release into the blood after the superhydrophobic surface contacted with blood for 24 h (Fig. S27). The in vitro cytotoxicity of the wax@PTL coating was further evaluated with a tetrazolium bromide reduction (MTT) cell viability assay of mouse fibroblast cells (3T3 cells). According to standard test procedures (GB/T 16886.5-2017, GB/T 16886.12-2017/ISO 10993-12:2012), Dulbecco's modified Eagle medium (DMEM) was prepared with an extract solution of the wax@PTL superhydrophobic material to culture the 3T3 cells. Different extraction amount was quantified by immersing modified glass at given area in 1 mL DEME, e.g., 6 cm^2/mL in Fig. 4f represented that the extract solution was prepared by immersing 6 cm^2 modified glass in 1 mL DEME. The corresponding viability of the 3T3 cells showed no significant difference from that of the 3T3 cells on the control DMEM solution after culturing for 72 h, which demonstrated that the wax@PTL material was not toxic to mouse fibroblast cells (Fig. 4f). The good blood compatibility was also reflected by a low adsorption of serum proteins and platelets (Fig. 4g). By using fluorescein isothiocyanate-labelled bovine serum albumin (BSA-FITC) as a model protein (a major component in serum), it was found that the wax@PTL coating surface had no obvious non-specific adsorption of BSA after incubating the wax@PTL coating in a 2 mg/mL BSA-FITC solution for 12 h, as observed from both the corresponding fluorescent spectra and images (Fig. 4h, i). Moreover, the WCA of the wax@PTL coating after incubation in the BSA solution at different time was still above 150° (Fig. 4j). The good resistance to the non-specific adsorption of serum proteins helped to further inhibit platelet adhesion and subsequently decrease the risk of blood clots [53]. It was noticeably observed that there were no platelets on the wax@PTL surface, while a large number of platelets were found on the bare silicon surface (Fig. 4k, l). The resistance to platelet adhesion was also ascribed to the low effective contact area available to platelets on the superhydrophobic wax@PTL coating surface. According to a possible Cassie
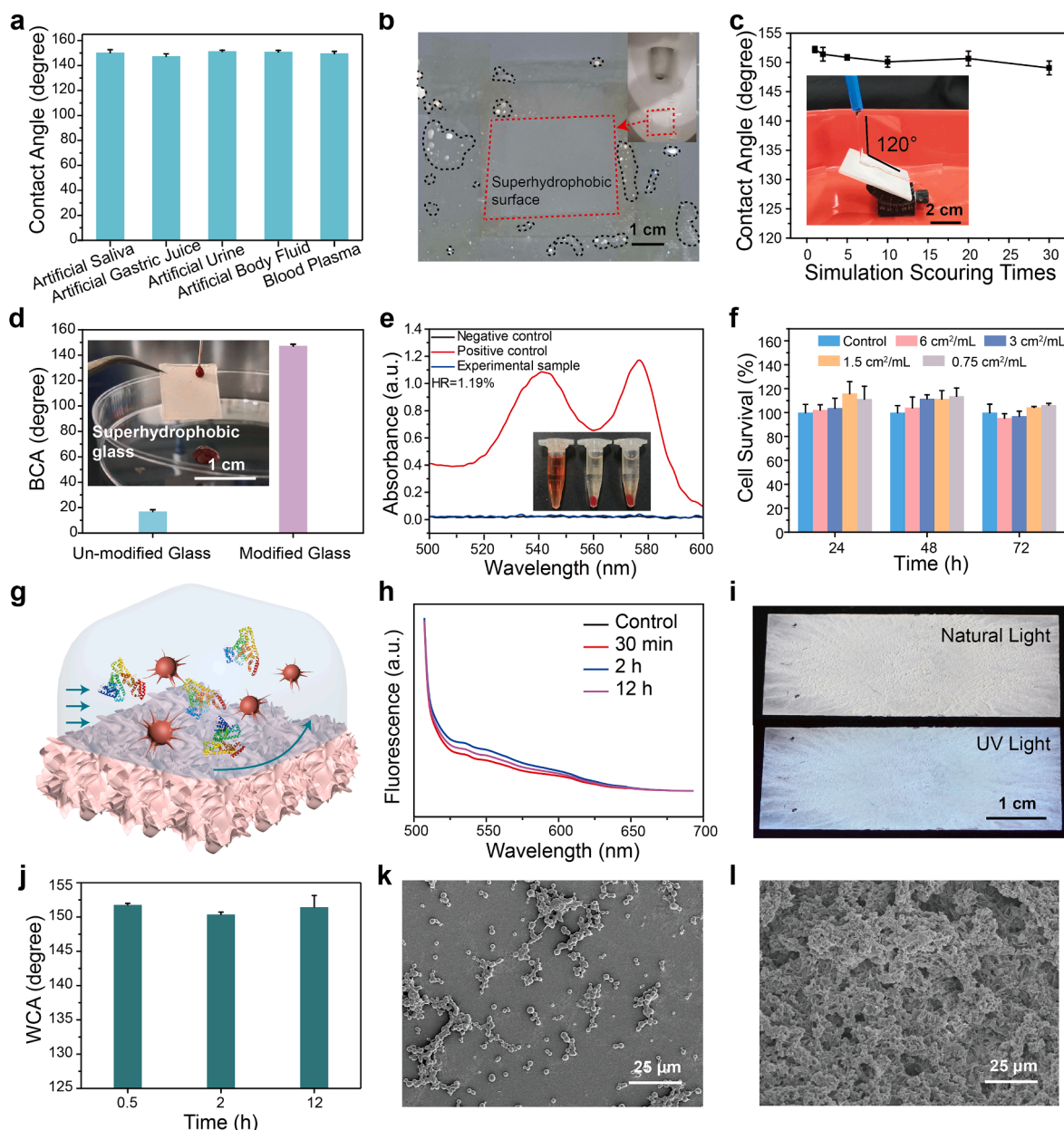
Fig. 4. (a) Contact angle of different biofluids on the superhydrophobic surface. (b) Superhydrophobic surface on a toilet (inset) showing resistance to the adherence of human urine. (c) Contact angle of artificial urine on the superhydrophobic surface after flushing with artificial urine for different times at an angle of 120°, as shown in the inset. (d) BCA on the un-modified and superhydrophobic glass, the inset shows that there was no visible trace of blood residue on the superhydrophobic glass. (e) Hemolysis assay of the positive control (left inset), experimental sample (middle inset) and negative control (right inset), as well as the corresponding UV/vis absorption curves. (f) Cytotoxicity of the superhydrophobic coating. (g) Schematic illustration of the superhydrophobic surface repelling the adhesion of platelets and proteins. (h) Fluorescence spectrum of the superhydrophobic surface before and after adsorbing BSA-FITC for different time. (i) Optical photo of the super-hydrophobic surface after the adsorption of BSA-FITC for 12 h under natural light and ultraviolet light. (j) WCA on the superhydrophobic surface after the adsorption of BSA-FITC. SEM images showing the platelet adhesion on the (k) blank silicon wafer and (l) modified surface.

state (Fig. S28) [14], when the blood was in contact with the super-hydrophobic surface, the liquid did not fill the rough grooves where air was trapped, thus reducing the available adhesion area for the platelets and protein.

3.5. Preparation of the blood-repellent wax@PTL coating on non-planar substrates

Unlike conventional blood-repellent materials typically using fluoroalkanes, the good biocompatibility of the wax@PTL is competitive advantage towards blood-repellent application in human. The noticeable resistance to the adhesion of blood on medical-grade materials (e.

g., gloves, blood storage bags) could effectively prevent contamination and infection for enhancing biological safety. Until now, most superhydrophobic materials are constructed on the surface of flat substrates, and it is still a major challenge to fabricate superhydrophobic coatings on specially shaped materials such as transfusion tubes [14]. Alternatively, another advantage of the method in this study is easy applicability on non-planar substrates. To achieve this purpose, the PTL nanofilm was first formed on the inner surface of a tube by immersing the tube in a buffer solution of lysozyme and cysteine for 2 h [40]. After staining with Congo Red (a dye that can specifically bind to amyloid structures), it was clearly revealed that the inner surface of the tube was successfully coated with the PTL nanofilm and that the amyloid

structures existed inside (Fig. S29). The PTL nanofilm coating had an average thickness of 161 ± 2 nm based on ellipsometry measurements and made the WCA of the silicon surface increase from the original 23 to 76° (Fig. S30). The superhydrophobic blood-repellent surface was then formed by soaking the PTL nanofilm-coated tube in a hexane solution of carnauba wax for a given time (Fig. 5a). By hexane evaporation-induced wax aggregation, a micro-/nano-scale topography was formed on the coating surface where the PTL nanofilm served as an intermediate layer to enhance the interfacial adhesion between the wax and substrate due to the supramolecular interaction (Fig. S31). The resulting BCA on the inner surface of the modified tube reached 150° (Fig. 5b). Subsequently, after transferring blood through the modified tube, no visible trace of blood contamination was detected on the superhydrophobic tube, while on the control tube, blood droplets visually adhered (Fig. 5c, d, Movie S6). In addition to the transfusion tube, the method in this study was also applicable for coating a blood storage bag (Fig. S32), in which the BCA on the inner surface of the modified blood storage bag could reach up to 151° without any blood residue being observed (Fig. 5e, f, Movie S6). In addition, the same method was used to modify a 3D-printed resin with a BCA of 150°, indicating the applicability of this method to the interior space of a device with a complex shape and morphology (Fig. 5g, S33).

4. Conclusion

In conclusion, we synthesized an all-natural superhydrophobic interfacial material in a green, energy-saving, and low-cost process. The PTL basement layer was simply obtained from a rapid phase transition of lysozyme that was stimulated by a non-toxic reducing agent (cysteine) through the thiol-disulfide exchange reaction. The PTL layer composing of a micro-/nano-scale topography could attach to virtually arbitrary material surface by a multiple binding mode due to the existence of adhesive amyloid-like structures inside the PTL. Subsequently, the PTL layer was coated by carnauba wax through spin, spray or dip coating, to achieve the facile production of a superhydrophobic material. The enriched functional groups of the PTL could interact with the hydrophobic component by hydrogen bonding to enhance the stability and hydrophobicity of the coating; furthermore, the coating would even maintain its superhydrophobicity after mechanical rubbing, bending or dynamic flushing by water.

The resulting superhydrophobic surface could impart cellulose-based packaging materials with water repellence and mold-proof properties, as well as providing the ability to resist the adhesion of food residues and biofluids (blood, urine, etc.) with a decrease in platelet adhesion. In addition, the all-natural superhydrophobic surface exhibited non-toxicity and excellent blood compatibility and could easily coat on the
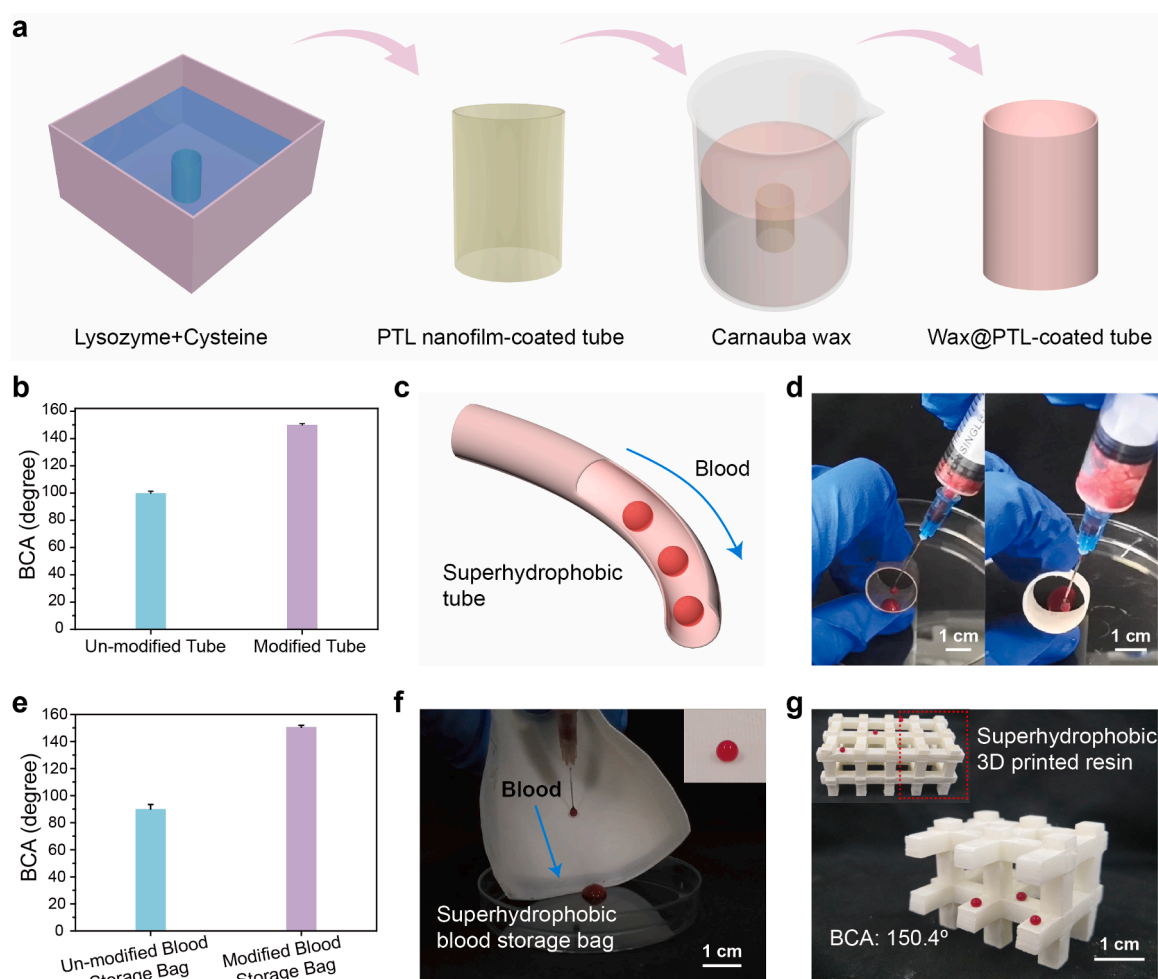

Fig. 5. (a) Schematic illustration for the formation of the superhydrophobic blood-repellent tube. (b) BCA on the un-modified and modified tubes. (c) Schematic illustration of the blood droplets rolling off from the superhydrophobic tube. (d) Images of the blood residues on the un-modified (left) and superhydrophobic blood-repellent (right) tubes after transferring blood through these tubes. (e) BCA on the un-modified and modified blood storage bags. (f) Images showing the blood residues and blood droplet on the superhydrophobic blood storage bag (inset). (g) Blood droplets on the inner surface of the modified 3D-printed resin. The inest shows a part of the 3D-printed resin (indicated by a red rectangle) was cutted and the corresponding exposed interior surface to repel the blood was shown in (g). (For interpretation of the references to color in this figure legend, the reader is referred to the web version of this article.)

interior spaces of non-flat substrates (e.g., tube, 3D-printed resin). Considering the low cost of materials (less than 0.0001 US dollars for the coating at 1 cm^2) and simple processing procedure, this method shows promise for large-scale application, thereby showing great potential for the development of recyclable packaging materials and biocompatible blood-contacting materials.

Declaration of Competing Interest

The authors declare that they have no known competing financial interests or personal relationships that could have appeared to influence the work reported in this paper.

Acknowledgements

Appendix A. Supplementary data

Supplementary data to this article can be found online at https://doi.org/10.1016/j.cej.2020.128347.

References

[1] H.J. Ensikat, P. Ditsche-Kuru, C. Neinhuis, W. Barthlott, Superhydrophobicity in perfection: the outstanding properties of the lotus leaf. Beilstein J. Nanotechnol. 2 (2011) 152–161.

[2] S. Naderizadeh, J.A. Heredia-Guerrero, G. Caputo, S. Grasselli, A. Malchiodi, A. Athanassiou, I.S. Bayer, Superhydrophobic coatings from beeswax-in-water emulsions with latent heat storage capability, Adv. Mater. Interfaces 6 (2019) 1801782–1801792.

[3] C.R. Reshmi, S.P. Sundaran, A. Juraij, S. Athiyanathil, Fabrication of superhydrophobic polycaprolactone/beeswax electrospun membranes for high-efficiency oil/water separation, RSC Adv. 7 (2017) 2092–2102.

[4] S. Wang, L. Jiang, Definition of superhydrophobic states, Adv. Mater. 19 (2007) 3423–3424.

[5] T. Kamegawa, Y. Shimizu, H. Yamashita, Superhydrophobic surfaces with photocatalytic self-cleaning properties by nanocomposite coating of TiO$_2$ and polytetrafluoroethylene, Adv. Mater. 24 (2012) 3697–3700.

[6] G.D. Bixler, B. Bhushan, Fluid drag reduction and efficient self-cleaning with rice leaf and butterfly wing bioinspired surfaces, Nanoscale 5 (2013) 7685–7710.

[7] J.A. Howarter, J.P. Youngblood, Self-cleaning and next generation anti-fog surfaces and coatings, Macromol. Rapid Commun. 29 (2008) 455–466.

[8] P.G. Pawar, R. Xing, R.C. Kambale, A.M. Kumar, S. Liu, S.S. Latthe, Polystyrene assisted superhydrophobic silica coatings with surface protection and self-cleaning approach, Prog. Org. Coat. 105 (2017) 235–244.

[9] S.S. Latthe, R.S. Sutar, V.S. Kodag, A.K. Bhosale, A.M. Kumar, K.K. Sadasivuni, R. Xing, S. Liu, Self-cleaning superhydrophobic coatings: potential industrial applications, Prog. Org. Coat. 128 (2019) 52–58.

[10] S.P. Dalawai, M.A. Saad Aly, S.S. Latthe, R. Xing, R.S. Sutar, S. Nagappan, C.-S. Ha, K. Kumar Sadasivuni, S. Liu, Recent advances in durability of superhydrophobic self-cleaning technology: a critical review, Prog. Organ. Coat. 138 (2020) 105381, https://doi.org/10.1016/j.porgcoat.2019.105381.

[11] X. Gao, X. Yan, X. Yao, L. Xu, K. Zhang, J. Zhang, B. Yang, L. Jiang, The dry-style antifogging properties of mosquito compound eyes and artificial analogues prepared by soft lithography, Adv. Mater. 19 (2007) 2213–2217.

[12] L. Wang, Q. Gong, S. Zhan, L. Jiang, Y. Zheng, Robust anti-icing performance of a flexible superhydrophobic surface, Adv. Mater. 28 (2016) 7729–7735.

[13] L. Cao, A.K. Jones, V.K. Sikka, J. Wu, D. Gao, Anti-icing superhydrophobic coatings, Langmuir 25 (2009) 12444–12448.

[14] S.S. Latthe, R.S. Sutar, A.K. Bhosale, S. Nagappan, C. Ha, K.K. Sadasivuni, S. Liu, R. Xing, Recent developments in air-trapped superhydrophobic and liquid-infused slippery surfaces for anti-icing application, Prog. Org. Coat. 137 (2019) 105373–105381.

[15] V. Jokinen, E. Kankuri, S. Hoshian, S. Franssila, R.H.A. Ras, Superhydrophobic blood-repellent surfaces, Adv. Mater. 30 (2018) 1705104–1705113.

[16] Z. Li, A. Milionis, Y. Zheng, M. Yee, L. Codispoti, F. Tan, D. Poulikakos, C.H. Yap, Superhydrophobic hemostatic nanofiber composites for fast clotting and minimal adhesion, Nat. Commun. 10 (2019) 5562–5572.

[17] S. Movafaghi, V. Leszczak, W. Wang, J.A. Sorkin, L.P. Dasi, K.C. Popat, A.K. Kota, Hemocompatibility of superhemophobic titania surfaces, Adv. Healthcare Mater. 6 (4) (2017) 1600717, https://doi.org/10.1002/adhm.201600717.

[18] L. Feng, Z. Zhang, Z. Mai, Y. Ma, B. Liu, L. Jiang, D. Zhu, A super-hydrophobic and super-oleophilic coating mesh film for the separation of oil and water, Angew. Chem. Int. Ed. 43 (2004) 2012–2014.

[19] W. Zhang, Z. Shi, F. Zhang, X. Liu, J. Jin, L. Jiang, Superhydrophobic and superoleophilic pvdf membranes for effective separation of water-in-oil emulsions with high flux, Adv. Mater. 25 (2013) 2071–2076.

[20] Y. Cai, L. Lin, Z. Xue, M. Liu, S. Wang, L. Jiang, Filefish-inspired surface design for anisotropic underwater oleophobicity, Adv. Funct. Mater. 24 (2014) 809–816.

[21] J.H. Kim, A. Mirzaei, H.W. Kim, S.S. Kim, Facile fabrication of superhydrophobic surfaces from austenitic stainless steel (AISI 304) by chemical etching, Appl. Surf. Sci. 439 (2018) 598–604.

[22] J.M. Lim, G.R. Yi, J.H. Moon, C.J. Heo, S.M. Yang, Superhydrophobic films of electrospun fibers with multiple-scale surface morphology, Langmuir 23 (2007) 7981–7989.

[23] X. Yao, L. Xu, L. Jiang, Fabrication and characterization of superhydrophobic surfaces with dynamic stability, Adv. Func. Mater. 20 (2010) 3343–3349.

[24] T. Darmanin, E.T. de Givenchy, S. Amigoni, F. Guittard, Superhydrophobic surfaces by electrochemical processes, Adv. Mater. 25 (2013) 1378–1394.

[25] P.S. Tsai, Y.M. Yang, Y.L. Lee, Fabrication of hydrophobic surfaces by coupling of langmuir-blodgett deposition and a self-assembled monolayer, Langmuir 22 (2006) 5660–5665.

[26] W.H. Huang, C.S. Lin, Robust superhydrophobic transparent coatings fabricated by a low-temperature sol–gel process, Appl. Surf. Sci. 305 (2014) 702–709.

[27] T.N. Van, Y.K. Lee, J. Lee, J.Y. Park, Tuning hydrophobicity of tio 2 layers with silanization and self-assembled nanopatterning, Langmuir 29 (2013) 3054–3060.

[28] W. Feng, L. Li, X. Du, A. Welle, P.A. Levkin, Single-step fabrication of high-density microdroplet arrays of low-surface-tension liquids, Adv. Mater. 28 (2016) 3202–3208.

[29] S. Pan, A.K. Kota, J.M. Mabry, A. Tuteja, Superomniphobic surfaces for effective chemical shielding, J. Am. Chem. Soc. 135 (2) (2013) 578–581, https://doi.org/10.1021/ja310517s.

[30] N. Johansson, A. Fredriksson, P. Eriksson, Neonatal exposure to perfluorooctane sulfonate (PFOS) and perfluorooctanoic acid (PFOA) causes neurobehavioural defects in adult mice, NeuroToxicol. 29 (2008) 160–169.

[31] A. Milionis, C.S. Sharma, R. Hopf, M. Uggowitzer, I.S. Bayer, D. Poulikakos, Engineering fully organic and biodegradable superhydrophobic materials, Adv. Mater. Interfaces 6 (1) (2019) 1801202, https://doi.org/10.1002/admi.201801202.

[32] R. Cai, K. Glinel, D.D. Smet, M. Vanneste, N. Mannu, B. Kartheuser, B. Nysten, A. M. Jonas, Environmentally friendly super-water-repellent fabrics prepared from water-based suspensions, ACS Appl. Mater. Interfaces 10 (2018) 15346–15351.

[33] S.M.R. Razavi, J. Oh, S. Sett, L. Feng, X. Yan, M.J. Hoque, A. Liu, R.T. Haasch, M. Masoomi, R. Bagheri, N. Miljkovic, Superhydrophobic surfaces made from naturally derived hydrophobic materials, ACS Sustain. Chem. Eng. 5 (2017) 11362–11370.

[34] W. Wang, K. Lockwood, L.M. Boyd, M.D. Davidson, S. Movafaghi, H. Vahabi, S. R. Khetani, A.K. Kota, Superhydrophobic coatings with edible materials, ACS Appl. Mater. Interfaces 8 (29) (2016) 18664–18668, https://doi.org/10.1021/acsami.6b06958.s003.

[35] Y. Li, J. Bi, S. Wang, T. Zhang, X. Xu, H. Wang, S. Cheng, B. Zhu, M. Tan, Bio-inspired edible superhydrophobic interface for reducing residual liquid food, J. Agric. Food Chem. 66 (2018) 2143–2150.

[36] Y. Zhang, J. Bi, S. Wang, Q. Cao, Y. Li, J. Zhou, B. Zhu, Functional food packaging for reducing residual liquid food: thermo-resistant edible super-hydrophobic coating from coffee and beeswax, J. Colloid Interface Sci. 533 (2019) 742–749.

[37] B. Liu, C. Xue, Q. An, S. Jia, M. Xu, Fabrication of superhydrophobic coatings with edible materials for super-repelling non-Newtonian liquid foods, Chem. Eng. J. 371 (2019) 833–841.

[38] I.S. Bayer, Superhydrophobic coatings from ecofriendly materials and processes: a review, Adv. Mater. Interfaces 7 (13) (2020) 2000095, https://doi.org/10.1002/admi.202000095.

[39] Y. Shen, Z. Wu, J. Tao, Z. Jia, H. Chen, S. Liu, J. Jiang, Z. Wang, Spraying preparation of eco-friendly superhydrophobic coatings with ultralow water adhesion for effective anticorrosion and antipollution, ACS Appl. Mater. Interfaces 12 (2020) 25484–25493.

[40] Y. Xu, Y. Liu, X. Hu, R. Qin, H. Su, J. Li, P. Yang, The synthesis of a 2D ultra-large protein supramolecular nanofilm by chemoselective thiol–disulfide exchange and its emergent functions, Angew. Chem. Int. Ed. 132 (2020) 2872–2881.

[41] C. Li, L. Xu, Y. Zuo, P. Yang, Tuning protein assembly pathways through superfast amyloid-like aggregation, Biomater. Sci. 6 (2018) 836–841.

[42] D. Wang, Y. Ha, J. Gu, Q. Li, L. Zhang, P. Yang, 2D protein supramolecular nanofilm with exceptionally large area and emergent functions, Adv. Mater. 28 (2016) 7414–7423.

[43] A. Gao, Q. Wu, D. Wang, Y. Ha, Z. Chen, P. Yang, A superhydrophobic surface templated by protein self-assembly and emerging application toward protein crystallization, Adv. Mater. 28 (2016) 579–587.

[44] J. Gu, S. Miao, Z. Yan, P. Yang, Multiplex binding of amyloid-like protein nanofilm to different material surfaces, Colloid Interface Sci. Commun. 22 (2018) 42–48, https://doi.org/10.1016/j.colcom.2017.11.009.

[45] C.A.S. de Freitas, P.H.M. de Sousa, D.J. Soares, J.Y.G. da Silva, S.R. Benjamin, M.I. F. Guedes, Carnauba wax uses in food – a review, Food Chem. 291 (2019) 38–48.

[46] H. Yu, N. Rouelle, A. Qiu, J. Oh, D.M. Kempaiah, J.D. Whittle, M. Aakyiir, W. Xing, J. Ma, Hydrogen bonding-reinforced hydrogel electrolyte for flexible, robust, and

all-in-one supercapacitor with excellent low-temperature tolerance, ACS Appl. Mater. Interfaces 12 (2020) 37977–37985.

[47] Z. Dai, Z. Feng, C. Feng, L. Meng, C. Li, C. Wang, L. Han, Y. Bai, Thermoplastic polyurethane elastomer induced shear piezoelectric coefficient enhancement in bismuth sodium titanate-PVDF composite films, J Appl. Polym. Sci. (2020), https://doi.org/10.1002/app.49818.

[48] Y. Lu, S. Sathasivam, J.L. Song, C.R. Crick, C.J. Carmalt, I.P. Parkin, Robust self-cleaning surfaces that function when exposed to either air or oil, Science 347 (2015) 1132–1135.

[49] Y. Wu, X. Luo, W. Li, R. Song, J. Li, Y. Li, B. Li, S. Liu, Green and biodegradable composite films with novel antimicrobial performance based on cellulose, Food Chem. 197 (2016) 250–256.

[50] Q. Wen, F. Guo, F. Yang, Z. Guo, Green fabrication of coloured superhydrophobic paper from native cotton cellulose, J. Colloid Interface Sci. 497 (2017) 284–289.

[51] M. He, M. Xu, L. Zhang, Controllable stearic acid crystal induced high hydrophobicity on cellulose film surface, ACS Appl. Mater. Interfaces 5 (2013) 585–591.

[52] A. Baidya, M.A. Ganayee, S.J. Ravindran, K.C. Tam, S.K. Das, R.H.A. Ras, T. Pradeep, Organic solvent-free fabrication of durable and multifunctional superhydrophobic paper from waterborne fluorinated cellulose nanofiber building blocks, ACS Nano 11 (2017) 11091–11099.

[53] W. Zhan, X. Shi, Q. Yu, Z. Lyu, L. Cao, H. Du, Q. Liu, X. Wang, G. Chen, D. Li, J. L. Brash, H. Chen, Bioinspired blood compatible surface having combined fibrinolytic and vascular endothelium-like properties via a sequential coimmobilization strategy, Adv. Funct. Mater. 25 (2015) 5206–5213.